Prediction of stress-corrosion cracking using electrochemical noise measurements: A case study of carbon steels exposed to H_2O-CO-CO_2 environment

J.W. van der Merwe [a,b], M. du Toit [b,c], D.E.P. Klenam [a,d,*], M.O. Bodunrin [a]

[a] School of Chemical and Metallurgical Engineering, University of the Witwatersrand, Johannesburg, South Africa
[b] Department of Materials Science and Metallurgical Engineering, University of Pretoria, South Africa
[c] School of Mechanical, Materials and Mechatronics Engineering, University of Wollongong, Australia
[d] Academic Development Unit, Faculty of Engineering and the Built Environment, University of the Witwatersrand, Johannesburg, South Africa

ARTICLE INFO

Keywords:
Stress-corrosion cracking
Stress intensity factor
Carbon steel
Electrochemical Noise
Zero Resistance Ammeter

ABSTRACT

At 45 °C, the stress-corrosion cracking (SCC) threshold was determined using current response measurements when carbon steels were exposed to a 50 %CO-50 %CO_2-H_2O environment. These measurements were performed by introducing an external "crack wall" surface and measuring a fraction of the current flow between the crack tip and this external surface. The current flow was measured between this external surface and the crack tip, by insulating most of the double cantilever beam samples, and using a zero-resistance ammeter (ZRA) to measure the current. These measurements showed that the threshold for cracking determined with this method corresponded well with the K_{ISCC} value measured for the same system. Crack tip activity was also measured, but it was difficult to correlate the current response data with the crack propagation rates, because of the crack length measurement resolution. However, it was possible to indicate the increased crack tip activity when the stress intensity showed slight variations, or for threshold stress intensity increase rates. The technique confirms the estimation of stress-corrosion thresholds and can be used to evaluate the influence of parameters on cracking in the absence of high-resolution crack length detection instrumentation.

1. Introduction

Corrosion is detrimental to structural integrity in many industries where the material (structure) interacts with its environment [1–8]. The presence of corrosion and stresses (thermal or mechanical) is even more dire and serious, leading to stress corrosion cracking phenomenon. In the petrochemical industry it is common to find water contaminated with carbon monoxide and carbon dioxide gas mixtures [1–4,9]. During coal gasification, by-product water is formed, and this is typically re-used as cooling water in heat exchanger applications [10,11]. However, when carbon steels are exposed to such environments with the appropriate gas mixture and stress conditions, they can experience stress-corrosion cracking [1,2,12–14]. These stress-corrosion cracks initiate and grow when exposed to some threshold stress conditions [1,2,12,15]. Welded joints would typically experience relatively high stresses close to the

Abbreviations: DCB, Double Cantilever Beam; SCC, Stress Corrosion Cracking; XRF, X-ray Fluorescence; ZRA, Zero Resistance Ammeter measurement.

* Corresponding author.
E-mail address: desprimus@gmail.com (D.E.P. Klenam).

yield point of the steel, and these joints are commonly post-weld heat treated to ensure lower residual stresses and thereby minimise cracking [16]. With existing flaws or cracks, the stress conditions are described as stress intensity, and stress intensity thresholds for stress-corrosion can be determined. Evaluating the relationship between stress intensity and crack propagation rate is time consuming [6]. Therefore, if current response measurements could be used to evaluate the crack activity during loading to establish stress intensity threshold, it would be possible to obtain a clearer understanding of the cracking system. Firstly, it is necessary to determine whether it would be possible to define the stress intensity threshold based on current response measurements. Secondly, stress fluctuations seem to contribute to the cracking activity which would contribute to crack propagation. However, crack propagation measurements might not be sensitive enough to give an accurate indication of the interdependencies between stress intensity and crack tip activity since crack propagation rates are generally very slow. The use of electrochemical noise measurements have been used to estimate crack propagation rates of carbon steel exposed to water with varying types of gas mixtures [17–19]. Correlation between cracking and peaks in the noise measurements were determined, but their conditions were plant related [19]. This study considers the possibility of investigating the predictions of the stress intensity threshold by using current response techniques under laboratory conditions.

The measurements were identical to experiments performed on type 304 stainless steel in pure water [20]. The current response measurement technique was used to determine the stress intensity threshold for stress-corrosion to give an indicator of cracking. These types of measurements performed on cracked samples would be viable if the film rupture/ slip dissolution model for cracking exists for crack initiation and propagation in these systems. Several researchers have described the stress-corrosion of steel in H_2O-CO-CO_2 medium [15,21,22] as a typical film rupture/slip dissolution model with the carbon monoxide adsorbing on the steel surface to inhibit corrosion [23,24]. The following three options exist during this type of crack propagation: cathodic process is carried out within the boundaries of the crack, or the current is taken up either fractionally in the crack, or totally on the external surface [25]. Even if the last is true, current in the crack propagation rate should be seen flowing from the crack mouth to the external surfaces. When loading above the stress-corrosion cracking (SCC) stress intensity threshold, zero resistance ammeter measurements (ZRA) for crack propagation in engineering alloys in power plant conditions changed rapidly in the positive direction [20]. These measurements corresponded to a reversal in polarity due to activation of the crack tip, and the flow of positive current from the crack tip to the external surfaces. During stress-corrosion of sensitized 304 stainless steel in pure water at elevated temperatures, typical of light water reactors, current flows from a crack to an external cathode [20]. The cathodic reaction did not occur only on the crack flanks or crack mouth, but also on the external surfaces [25].

In the current study, the influence of cracking was investigated by applying an external surface to a compact tension sample and measuring the current flow with a ZRA between the sample and the external surface. The environmental system, gas composition and temperature were chosen that would sustain cracking [26]. This consisted of an A516 pressure vessel steel exposed to water with a 50 % carbon monoxide, 50 % carbon dioxide gas mixture pressurized to 800 kPa at 45 °C. The stress intensity threshold for SCC for this steel system was determined, and was relatively low, ~3 MPa$\sqrt{m}$ [27,28]. Only the stress intensity and loading circumstances were altered to establish the current response, with the ambient parameters remaining constant throughout the experiment.

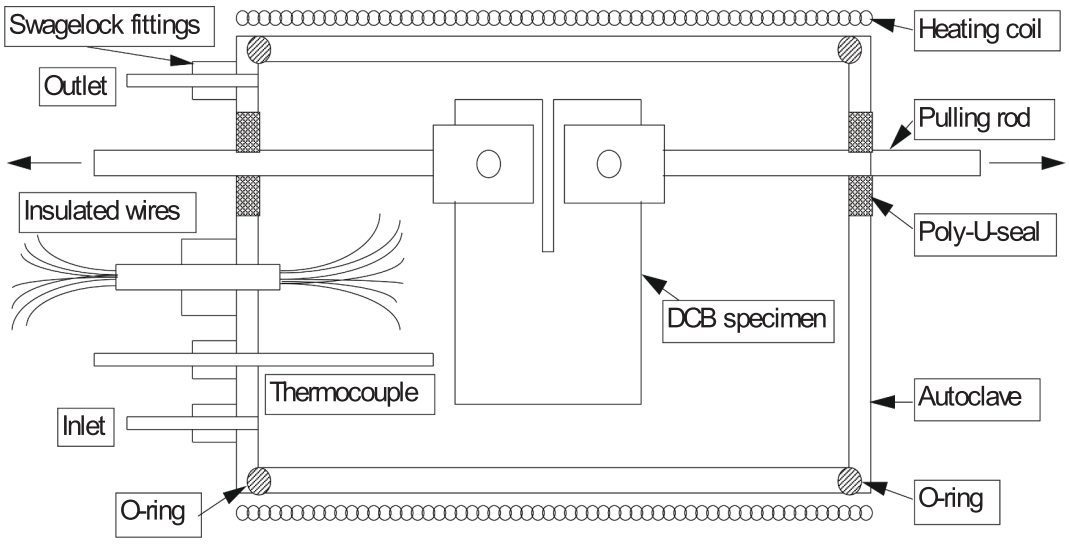

Fig. 1. Diagram of the autoclave in which the experiments were undertaken.

2. Materials and method

2.1. Specimen configuration and clamping

The current response measurements with stress intensities were evaluated using double cantilever beam (DCB) specimens. The DCB specimens were designed and machined by adapting the ASTM E399-22 standard [29]. The suitability of this specimen for stress corrosion cracking investigation was reported by Roy [29]. Fig. 1 shows the experimental set-up used to expose the double cantilever beam specimens to the environment in an autoclave.

The temperature of the test autoclave was maintained by a heating element positioned around the autoclave. To avoid the development of an electro-magnetic field, this heating element was folded back on itself so that the induced field did not alter the crack depth measurements.

A potential drop method was used to determine the crack length. This was accomplished by passing a 1A current through the sample and measuring the potential drop on the sample's top surface (as shown in the schematic diagram in Fig. 2) and at the crack's origin. The ratio of these two values was used to determine the length of the crack. Before the test, the setup was calibrated to determine the crack depth. Although the sample's dimensions were less than those required for a DCB specimen, the specimen's configuration conformed to linear elastic fracture mechanics due to the embrittling nature of the environment.

2.2. Environment conditions

Water-resistant silicon rubber was applied to the external surface of each compact stress specimen to protect it from the environment. Separate steel pieces were positioned in proximity on opposite sides of the crack to form a "new" external surface. The electrons generated at the crack tip were diverted to the new exterior surface through a ZRA. The compact specimen was electrically linked to the ZRA by attaching an insulated wire to the external surfaces and pulling it out of the autoclave in which the tests were performed.

The electrons went from the compact specimen via the ZRA and back to the cathodic surface, where they were involved in with reduction and oxidation reactions. The amount of current created during the electro dissolution process could be determined by inserting the no-loss current measuring device into the circuit. The conductivity of the water limited the distance over which positive current could flow as it passed through the crack opening, hence the "cathodes" were placed near to the crack mouth as illustrated in Fig. 3.

2.3. Steel sample

The A516 pressure vessel steel was used throughout the study, with the composition reported in Table 1. The compositions were analysed using Leco Carbon/Sulphur Analyzers, 3460 Emission Spectrometer, and were verified with the 8680 + 72RET XRF spectrometers.

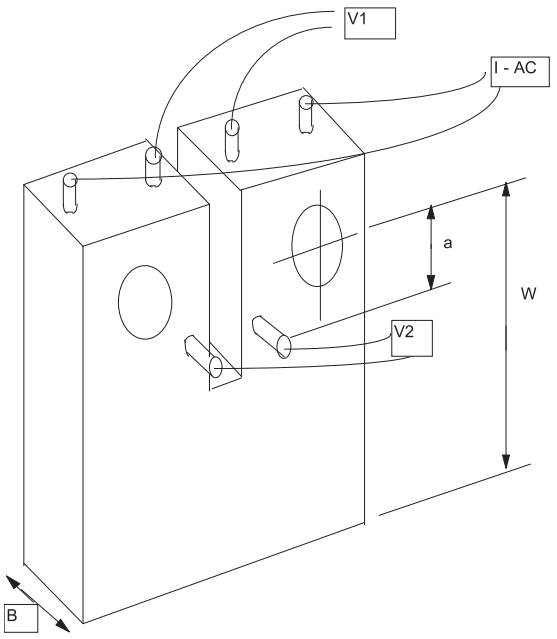

Fig. 2. Potential drop method used for the crack propagation measurement.

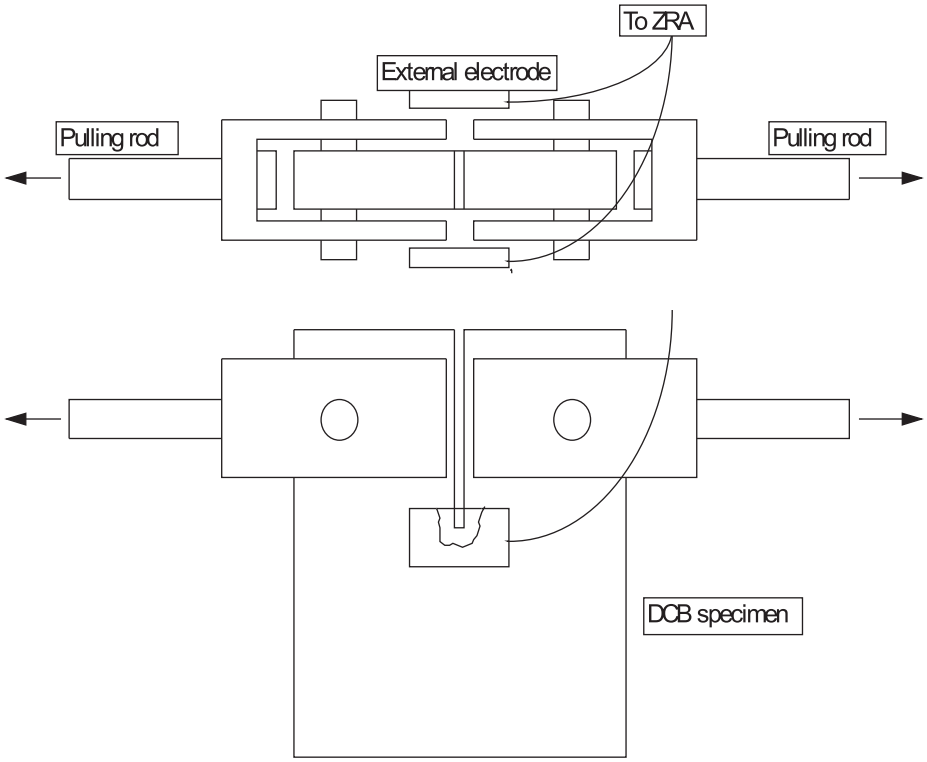

Fig. 3. The external electrode is shown in the schematic diagram of the double cantilever beam specimen.

Table 1
The composition of A516 pressure vessel steel.

Element	Al	B	C	Co	Cr	Cu	V	Mn
wt%	0.009	0.002	0.217	0.010	0.010	0.010	0.010	1.030
Element	Mo	N2	Nb	Ni	P	S	Ti	Si
wt%	0.010	0.007	0.004	0.020	0.009	0.003	0.001	0.290

2.4. Experimental procedure

Before the experiments, nitrogen was bubbled through the water in the pressure vessel for at least an hour to achieve a low total dissolved oxygen concentration. When high dissolved oxygen concentrations were detected, air was bubbled through the container until the desired level of 8 ppm was reached, which was confirmed using a dissolved oxygen meter. The CO-CO_2 gas mixture was then used to pressurize the water. The experiments were carried out at 45 °C or 25 °C, with the temperature being adjusted by external heating of the autoclave. With the 50 % CO-50 %CO_2 gas mixture, the vessel was pressurised to 800 kPa. The pressurized water was then released into the test autoclave.

Experiments were conducted at 25 °C and 45 °C using the potential drop crack measurement technique. The stress intensity was increased to a predetermined level from a low-load conditions. The predetermined stress intensity did not exceed 70 % of the expected peak intensity as recommended by Roy [29]. The stress level was maintained at this level for an extended period of at least 14 h. The stress intensity was then reduced to a low-load state for at least one hour, during which time the current response was measured. The response and all other measurements were taken every 20 s.

2.5. Fracture mechanics calculations

Compact tension specimens were utilized to assess the stress intensity in accordance with ASTM E399 – 90 [30]. The specimen's dimensions and configuration are shown in Fig. 4. The crack length was calibrated by introducing precise crack sizes while measuring the potential difference. This was done to avoid errors in the measured data.

Equations (1) and (2) were used to calculate K_Q for the compact specimens.

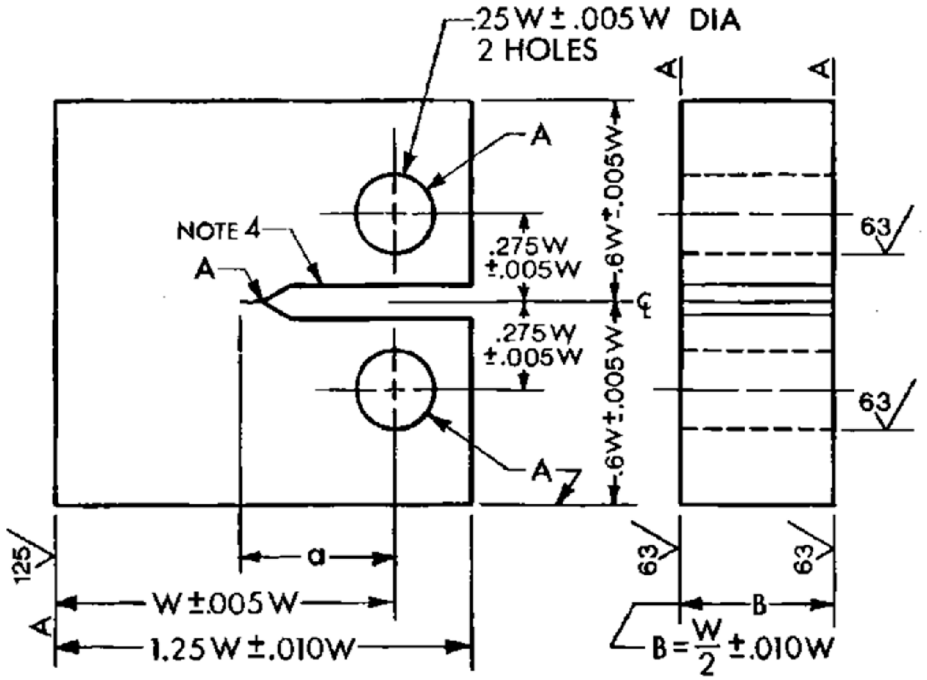

Fig. 4. Compact specimen, C(T) with standard proportions and tolerances (units are in mm).

$$\mathbf{K_Q} = \left(\frac{\mathbf{P_Q}}{\mathbf{B}\sqrt{\mathbf{W}}}\right).\mathbf{f}\left(\frac{\mathbf{a}}{\mathbf{W}}\right) \tag{1}$$

where: f(a/w) is given as:

$$\mathbf{f}\left(\frac{\mathbf{a}}{\mathbf{W}}\right) = \frac{(2+\frac{\mathbf{a}}{\mathbf{W}})(0.866+4.64\frac{\mathbf{a}}{\mathbf{W}}-13.32\frac{\mathbf{a}^2}{\mathbf{W}^2}+14.72\frac{\mathbf{a}^3}{\mathbf{W}^3}-5.6\frac{\mathbf{a}^4}{\mathbf{W}^4})}{(1-\frac{\mathbf{a}}{\mathbf{W}})^{\frac{3}{2}}} \tag{2}$$

where P_Q = load; B = specimen thickness; W = specimen width; a = crack length.

2.6. Determination of the stress intensity threshold

The tests were carried out for at least 14 h with constant load, and the crack propagation rates were calculated.

3. Results

The ZRA signal results were plotted against stress intensity and the crack growth rates were also shown. Different stress intensity

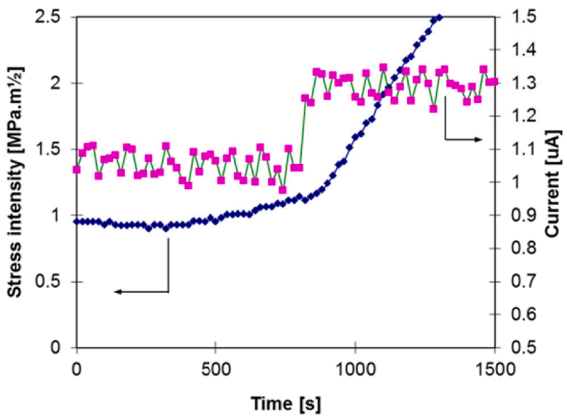

Fig. 5. Plot of stress intensity factor and the ZRA signal against time when stress intensity was below 3 MPa$\sqrt{m}$.

levels between the range of 1 and 60 MPa$\sqrt{m}$ were applied, and the effect of low (<3MPa$\sqrt{m}$) and high (>3MPa$\sqrt{m}$) stress intensities were evaluated. In addition to this, the effect of stress intensity increase rate was investigated at low and high stress intensities. Lastly, the correlation of the ZRA response with the measured crack propagation rate was investigated.

3.1. ZRA signal response at low levels of stress intensity

The stress intensity threshold for stress-corrosion for this system was 3 MPa.m$^{1/2}$, and this was used as a reference point for the evaluation of the current response signals. It was expected that the current response signal would show some change during load application as an indication of activity at the crack tip. At low stress intensity levels an increase in stress intensity caused an increase in the ZRA signal. Fig. 5 shows that when the stress intensity was kept constant at 1 MPa$\sqrt{m}$ and then gradually increased to 2.5 MPa$\sqrt{m}$, the ZRA signal increased as soon as the stress intensity increased above 1.2 MPa$\sqrt{m}$. The ZRA signal rose by roughly 0.25 μA, showing increasing activity at the crack tip. The fracture propagation rate could not be adequately measured at this tiny increase in stress intensity. Only when the stress intensity was elevated over 1.2 MPa$\sqrt{m}$did the ZRA signal increase, with constant amplitude.

Fig. 6 shows that the ZRA signal increased as the stress intensity increased from 1 MPa$\sqrt{m}$ to 30 MPa$\sqrt{m}$. As the stress intensity rose above ~ 3 MPa$\sqrt{m}$, the ZRA signal gradient increased. Although, the ZRA signal was not sensitive to the local minimum and local maximum of the stress intensity observed prior to the increase observed at > 12000 s.

In Fig. 7, the ZRA signal is plotted against time. The signal's amplitude was 0.05 μA. The ZRA signal increased in response to increasing stress intensity, with two increases seen: first, when the stress intensity was elevated to 4 MPa$\sqrt{m}$, and second, when it was raised over ~ 3 MPa$\sqrt{m}$. It rose to ~ 2.4 μA and then fluctuated after the initial rise. It reached ~ 2.55 μA with the second increment, but then dropped slightly when the stress intensity was reduced, and then fluctuated with constant stress intensity of 20 MPa$\sqrt{m}$.

3.2. ZRA response and the stress intensity increase rates

Results from slow strain-rate and cyclically loaded specimens showed that the strain rate near the crack tip had a significant impact on cracking. This phenomenon was examined to determine the impact of changing stress intensity rates. A rapid jump in the ZRA signal was observed in Fig. 8 when the stress intensity was increased to ~ 65 MPa$\sqrt{m}$ from 50 MPa$\sqrt{m}$. The rate at which the stress intensity was increased is most likely responsible for this increase. This greater ZRA signal lasted for about 10,000 s before dropping to the previous value at ~ 15000 s. At this point, there was no further increase in stress intensity as it was kept constant at ~ 70 MPa$\sqrt{m}$. Fig. 9 shows that the gradient of the stress intensity during the increase was 0.0036 MPa$\sqrt{m}$.s^{-1} when the increasing portion of the stress intensity curve was fitted linearly.

Fig. 10 shows the ZRA signal and stress intensity over time for a test performed at 25 °C. The amplitude and frequency of the ZRA signal increased as the stress intensity rose. The amplitude of the ZRA signal reduced when the loading rate decreased and the stress intensity steadied, and the signal's frequency decreased. The ZRA signal's mean current was steadily decreasing. Fig. 11 shows crack growth and demonstrates that the crack propagation rate was higher from 0 to 8 000 s than from 8 000 to 20 000 s, although the latter region still had a comparatively high crack propagation rate. The overall crack length can be estimated using the linear fit (black line) relationship in Fig. 11.

Another example of an increasing stress intensity condition is shown in Fig. 12. This test was performed at 25 °C, and there was therefore a slightly lower sensitivity to cracking. When the stress intensity was varied, the effect of loading rate on cracking was examined. Because of the modest influence of the measurements on the stress intensity, the measured crack length was not employed. When the crack length was examined more closely, however, crack expansion did occur. The ZRA signal reflected this as well. At some point the ZRA signal started to increase, and this continued throughout the increase of the stress intensity. However, when the stress intensity was dropped to zero, the current also showed a drop.

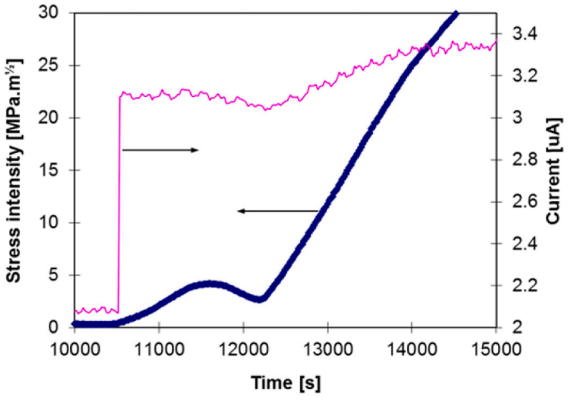

Fig. 6. Plot of stress intensity factor and the ZRA signal against time when stress intensity was increased up to 30 MPa.m1/2.

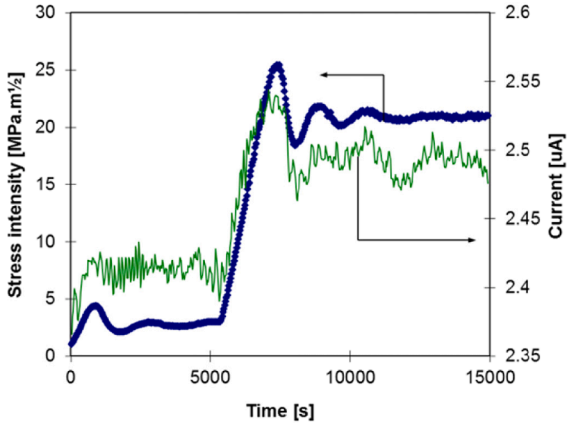

Fig. 7. Stress intensity and the ZRA signal plotted against time with amplitude signal of 0.5 μA.

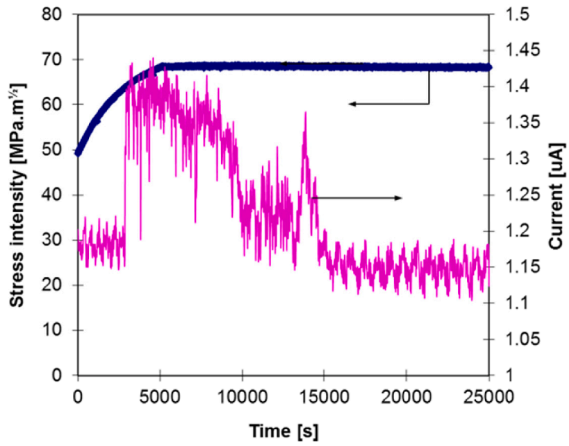

Fig. 8. Stress intensity and ZRA signal plotted against time showing the effect of initial increase in stress intensity.

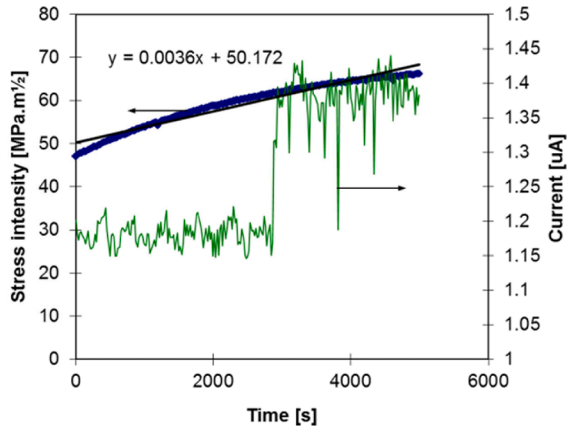

Fig. 9. Stress intensity factor and the ZRA signal plotted against time, showing increasing stress intensity fitted using a linear equation.

3.3. ZRA response as the stress intensity was lowered from high levels

The ZRA signal declined from ~ 1.15 to ~ 0.8 μA as the stress intensity was reduced from ~ 68 MPa$\sqrt{m}$ to ~ 3 MPa$\sqrt{m}$. The ZRA signal surged abruptly when the stress intensity fell below ~ 53 MPa. $\sqrt{m}$, then dropped drastically within 150 s. The ZRA response

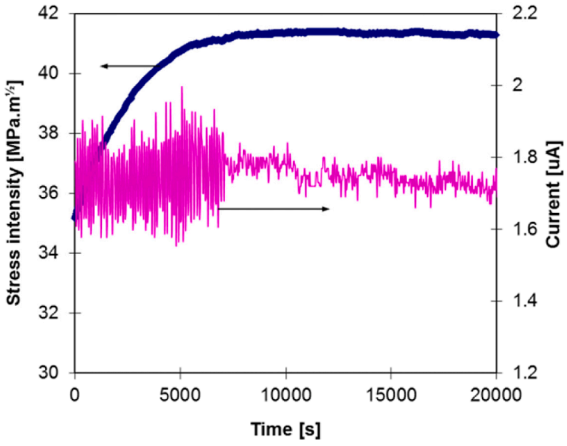

Fig. 10. Stress intensity and the ZRA signal plotted against time at 25 °C.

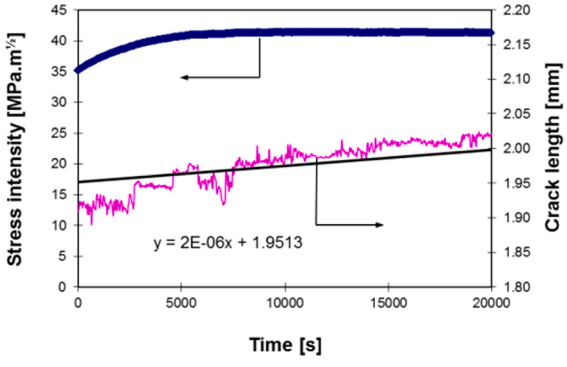

Fig. 11. Stress intensity and the measured crack growth plotted against time.

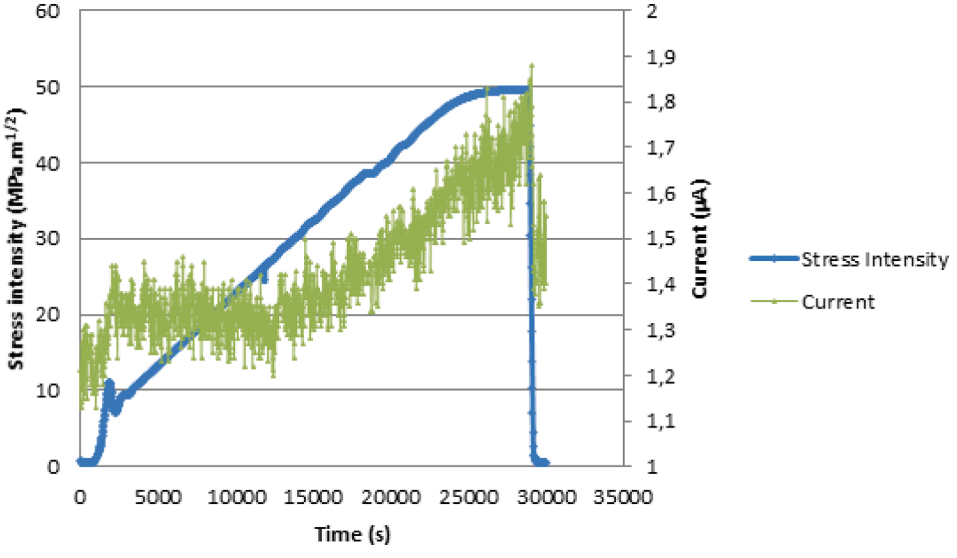

Fig. 12. Plot of stress intensity and the ZRA signal against time showing the effect of loading rate at 25 °C.

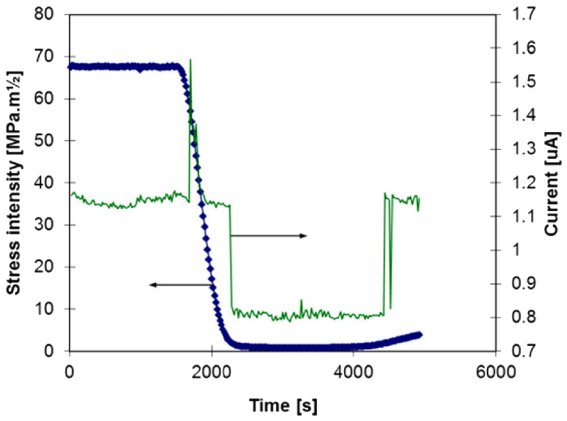

Fig. 13. Stress intensity and the ZRA signal plotted against time when stress intensity was lowered from ~68 MPa$\sqrt{m}$.

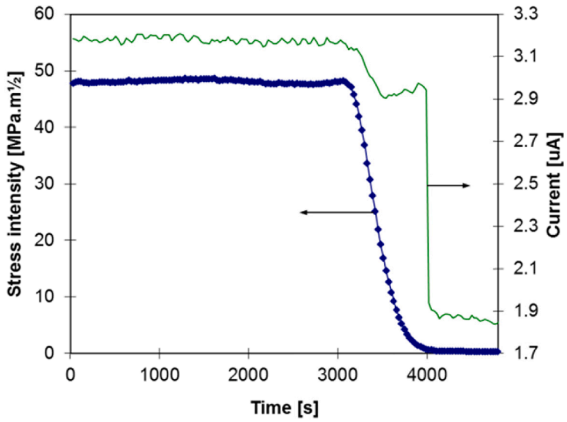

Fig. 14. Stress intensity and ZRA signal plotted against time when stress intensity was lowered from 48 MPa$\sqrt{m}$.

was also sensitive to the slight increase in stress intensity at about 4200 s.

Fig. 14 shows that as the stress intensity was reduced from 48 to 0 MPa$\sqrt{m}$, the ZRA signal decreased at a certain gradient, but when the stress intensity was reduced to 15 MPa$\sqrt{m}$, the gradient lowered significantly, and the mean value of the ZRA signal increased slightly again as the stress intensity was reduced. The ZRA signal declined sharply by 1 μA as the stress intensity dropped to ~ 0 MPa.$\sqrt{m}$.

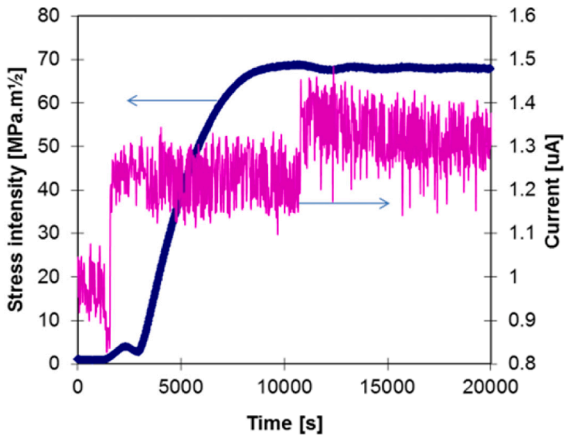

Fig. 15. Stress intensity factor and the ZRA signal shown against time with fluctuating stress levels.

3.4. ZRA response with fluctuations in stress intensity levels

In Fig. 15, the stress intensity was held constant at 1 MPa$\sqrt{m}$ before increasing to 4 MPa. $\sqrt{m}$. The load was applied after a slight drop to ~ 3 MPa$\sqrt{m}$ and the final stress intensity above ~ 65 MPa$\sqrt{m}$ was attained. The load was applied by temperature control of the testing frame. The frame consisted of two arms with electrical heaters placed inside. The zero-load condition was achieved by heating up these arms to a maximum temperature to ensure no load condition, and with no play to cause an increase in stress with the shrinkage of the arms as the temperature was lowered. By controlling the temperature of the arms, the stress could be controlled. When there was no load control, the stress intensity is plotted versus time together with the ZRA signal in Fig. 16. The load control on the specimen became unstable, and the stress intensity became unstable because of this loss of control. The amplitude and frequency of the ZRA signal increased due to the instability at 40 MPa$\sqrt{m}$. The amplitude of the signal was increased from 0.08 to approximately 0.14 μA. The ZRA signal recovered to its original proportions after this incidence of instability, although the frequency was still high.

With a changed stress intensity, the ZRA signal in Fig. 17 increased progressively from 2.4 to 2.65 μA. The stress level was maintained at ~ 20.4 MPa$\sqrt{m}$. The stress intensity then decreased to ~ 20.1 MPa. $\sqrt{m}$ before rising to ~ 20.4 MPa. $\sqrt{m}$.

3.5. ZRA response correlated with crack growth rates

In Fig. 18, the crack growth is plotted with a stress intensity of 15 MPa$\sqrt{m}$. The general trend of the crack length did not show any propagation up to the last fifth shown, where there was also a slight increase in the current response measurement (ZRA signal). However, the crack propagation rate did not show a significant correlation with the current response signal.

4. Discussion

4.1. Stress intensity threshold

Analysis of the data showed that the current response data could indicate the threshold for stress-corrosion. Although the threshold predicted by the current response was slightly lower than the determined K_{ISCC}, it still gave a conservative estimation. Therefore, the ZRA measurements were significant, and gave an indication of the activity at the crack tip. The stress intensity threshold appeared to be above 1.5 MPa$\sqrt{m}$ and below 7 MPa$\sqrt{m}$ (Figs. 5 - 7) The current reacted to changes in stress intensity and crack length in a variety of ways, including abrupt rises in increased and decreased mean values; changes in the amplitude; changes in frequency; the polarity; and the general gradient of the ZRA signal's mean value [5].

If the "slip-step dissolving model" is adopted, the abrupt increase in the ZRA signal for the detection of the cracking threshold value can be linked to this cracking system [20]. According to Manahan et al. [20], the fracture of the passive layer at the crack tip caused the increase in the ZRA signal, which is the only explanation for an increase in ZRA when the stress intensity was increased. However, according to the slip dissolution model, this would imply that crack propagation happens when the passive layer fractures, so as a result, an increase in the ZRA signals indicated the start of crack propagation.

In this study, the more occurrences of passive film rupture must have contributed to the total crack growth, as indicated by the higher frequency of the ZRA signals (Figs. 5 - 7). The increased amplitude could have reflected the magnitude of the events at the crack tip (Figs. 8 - 14). Manahan et al. [4] observed a greater amplitude following a time of incubation in which the fracture had to propagate through the highly strained pre-cracked zone, which they described as a higher crack growth rate. As the fracture length increased beyond this range, crack formation became easier, and the amplitude and frequency of the ZRA signal increased.

The sign of ZRA signal revealed the nature of the process occurring at the crack tip, allowing the mechanism producing cracking could be deduced. A positive ZRA signal was an indication that the resultant reaction at the crack tip was anodic, and a cathodic

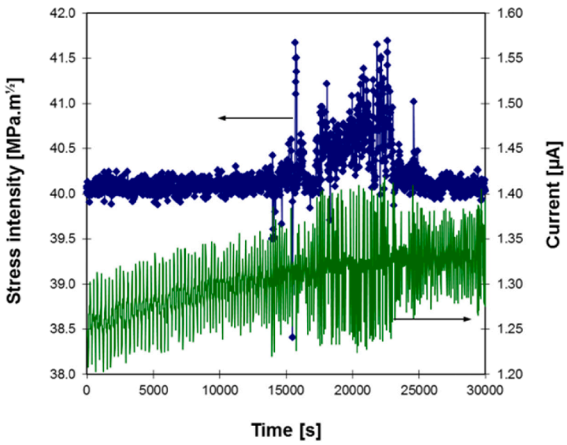

Fig. 16. Stress intensity and the ZRA signal plotted against time when there was no load control.

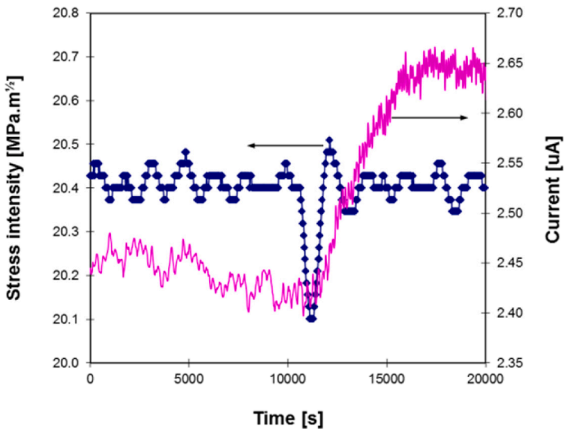

Fig. 17. Stress intensity and the ZRA signal plotted against time for the 25C, 50 % CO-CO_2 and 800 KPa.

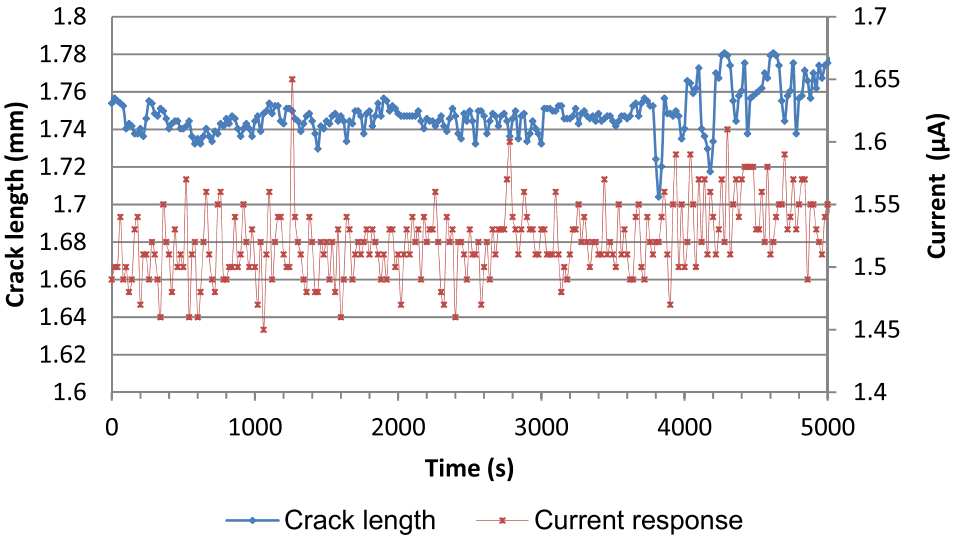

Fig. 18. Crack length and the ZRA signal plotted against time at constant stress intensity of 15 MPa.$m^{½}$.

reaction occurred on the artificial crack sides [5,31]. There were signal losses as not all signals could be measured and might have been lost during the measurement Due to possible fractional loss of current flow, it was challenging to quantify the overall current response as a crack propagation rate. Thus, the results are more of qualitative indication of crack tip activity.

4.2. Cracking-related factors revealed by current response measurements

According to research using potential drop crack measurement technique [15], crack propagation is influenced by a constant stress or stress intensity, as well as the rate the stress intensity increase. Thus, loading rates affect the initiation of cracking, making determining the stress intensity threshold at these conditions more difficult. This was confirmed by the discovery that fracture propagation was not solely influenced by stress severity [20] According to response data in this work, the loading rate, or the rate at which the stress intensity increased (Figs. 8 - 11), had a major impact on crack formation.

As the ZRA signal responded to the change in stress intensity (Fig. 15), it appeared that there was very high chance of cracking with significant increase in the current. This was most likely caused by the fracture of the passive layer, which resulted in a higher strain rate at the crack tip [20]. As the load was released (i.e., measurements taken under no load condition), the current response measurements showed an increase in frequency and amplitude (Fig. 16), and the stress intensity declined at a rate of 0.0036 MPa.$m^{1/2}$/s. This meant the likelihood of cracking increased during unloading, indicating that fracture propagation was dependent on loading rate. Thus, it was possible to detect when cracking started and when it stopped using the current response. This was observed when stress intensity changes resulted in higher current response fluctuations.

4.3 Limitations

From these results some weaknesses have been identified. Firstly, the difficulty in correlating the crack growth measurements with the ZRA signal response. With the potential drop crack measurement technique, the link between the current response and the crack propagation rate was not detectable (Fig. 18). Unfortunately, the fracture length measurements had poor resolution, making crack propagation below 50 μm difficult to detect. This meant the current response measurements provided a more sensitive indication of crack propagation than the crack propagation measurement. However, the current response measurements correspond to the activity at the crack tip which would occur at a relatively high crack tip deformation rate. The crack propagation rate was relatively slow at around 10^{-9} m.s^{-1} (10^{-6} mm.s^{-1} or 3.6 μm.h^{-1}), so it was difficult to correlate the two measurements (the crack growth rate measurement (potential drop measurement) and the current measurement), since the activity at the crack tip could be cyclical, as small bursts of crack growth. This was the expected growth pattern, and a continuous crack growth rate pattern was not seen [29]. Under cyclical stress conditions, these short growth bursts would probably be sustained at a higher frequency. Since the whole process is related to the corrosion and passivation rates, which are relatively slow, a maximum crack growth rate would exist when controlled by these electrochemical rates. Thus, the ZRA signal could not be effectively correlated as a direct indication of crack propagation. However, as cracking progressed, the amplitude of the ZRA signal increased, or the mean value increased abruptly, as in the case of stress intensity above the threshold. Although there were variations in the results, the trends were good for qualitative assessment of the process, especially for stress corrosion cracking of carbon steels in the selected media. Some of the inconsistencies are attributed to crevices formed between the steel and the silicon rubber insulation. This increased the noise in the measurements.

5 Conclusions

In this work, a new approach for determining the threshold of stress-corrosion cracking of carbon steels in H_2O-CO-CO_2 environment was investigated. Current response due to external “crack wall” surface was measured using zero-resistance ammeter. The following conclusions were drawn:

1. The current response measurements could be used to detect the stress intensity threshold for stress corrosion cracking.
2. The ZRA signal indicated that cracking had occurred, however there was no clear correlation between crack growth and the ZRA signal.
3. Current response measurements indicated the role of strain rate dependence of cracking since current response increased with increasing the strain rate.
4. There was inconsistency with the correlation of the crack length and electrochemical response. However, the ZRA signal increased with activity at the crack tip, corresponding with crack growth.

Declaration of Competing Interest

The authors declare that they have no known competing financial interests or personal relationships that could have appeared to influence the work reported in this paper.

Data availability

No data was used for the research described in the article.

Acknowledgements

Professors R.F. Sandenbergh, C. Pistorius and G.T. van Rooyen, all from the Department of Metallurgical Engineering, University of Pretoria, South Africa for their assistance and support during the project.

References

[1] E. Adu, Y. Zhang, D. Liu, Current situation of carbon dioxide capture, storage, and enhanced oil recovery in the oil and gas industry, Can. J. Chem. Eng. 97 (5) (2019) 1048–1076, https://doi.org/10.1002/cjce.23393.
[2] A. Chapoy, P. Ahmadi, V. de Oliveira Cavalcanti Filho, P. Jadhawar, “Vapour-liquid equilibrium data for the carbon dioxide (CO2) + carbon monoxide (CO) system,” J. Chem. Thermodynam., vol. 150, Nov. 2020, doi: 10.1016/j.jct.2020.106180.
[3] E. E. Heaver and R. F. Sandenbergh, “Inhibition of stress corrosion cracking of carbon manganese steels in the CO2-H2O system,” in Progress in the Understanding and Prevention of Corrosion, J. M. Costa and A. D. Mercer, Eds. 1993, pp. 1562–1572.
[4] W.J. Lochmann, Materials problems in coal gasification and liquefaction, Metall. Trans. A 9 (2) (1978) 175–181.
[5] J.W. van der Merwe, The stress-corrosion cracking of carbon steel in CO-CO2-H20, University of Pretoria, Pretoria, 2013.
[6] D.E.P. Klenam, L.H. Chown, M.J. Paoo, L.A. Cornish, Steels for rail axles - an overview, Crit. Rev. Solid State Mater. Sci. (2022), https://doi.org/10.1080/10408436.2022.2137462.
[7] M.O. Bodunrin, L.H. Chown, J.W. van der Merwe, K.K. Alaneme, C. Oganbule, D.E.P. Klenam, N.P. Mphasha, Corrosion behavior of titanium alloys in acidic and saline media: role of alloy design, passivation integrity, and electrolyte modification, Corros. Rev. 38 (1) (2020) 25–47, https://doi.org/10.1515/corrrev-2019-0029.
[8] D.E.P. Klenam, M.O. Bodunrin, S. Akromah, E. Gikunoo, A. Andrews, F. McBagonluri, Ferrous materials degradation: characterisation of rust by colour – an overview, Corros. Rev. 39 (4) (2021) 297–311, https://doi.org/10.1515/corrrev-2021-0005.

[9] R. de Motte, et al., A study by electrochemical impedance spectroscopy and surface analysis of corrosion product layers formed during CO2 corrosion of low alloy steel, Corros Sci 172 (2020), 108666.
[10] G. Oh, et al., Syngas production through gasification of coal water mixture and power generation on dual-fuel diesel engine, J. Energy Inst. 92 (2) (2019) 265–274.
[11] L. Wei, X. Pang, K. Gao, Corrosion of low alloy steel and stainless steel in supercritical CO2/H2O/H2S systems, Corros. Sci. 111 (2016) 637–648, https://doi.org/10.1016/j.corsci.2016.06.003.
[12] M. Kowaka, S. Nagata, Stress corrosion cracking of mild and low alloy steels in CO-CO2-H2O environments, Corrosion 32 (10) (1976) 395–401.
[13] A. Brown, J.T. Harrison, R. Wilkins, Trans-granular stress corrosion cracking (SCC) of ferritic steels, Corros. Sci. 10 (7) (1970) 547–548.
[14] A. Brown, J.T. Harrison, R. Wilkins, Investigations of stress corrosion cracking of plain carbon steel in the carbon dioxide -carbon monoxide - water system, in: In Conference on the Stress Corrosion CrackIng and Hydrogen Embrittlement of Iron Base Alloys, 1979, pp. 686–695.
[15] J.W. van der Merwe, M. du Toit, D.E.P. Klenam, M.O. Bodunrin, Fracture Mechanics of Carbon Steel Under Different Carbon Monoxide and Dioxide Gas Mixture Conditions in Water, Sci. Afr. 17 (2022) e01355, https://doi.org/10.1016/j.sciaf.2022.e01355.
[16] D.E.P. Klenam, G.S. Ogunwande, T. Omotosho, B. Ozah, N.B. Maledi, S.I. Hango, A.A. Fabuyide, L. Mohlala, J.W. van der Merwe, M.O. Bodunrin, Welding of magnesium and its alloys: an overview of methods and process parameters and their effects on mechanical behaviour and structural integrity of the welds, Manuf. Rev. 8 (29) (2021) 1–31, https://doi.org/10.1051/mfreview/2021028.
[17] C.A. Loto, Stress corrosion cracking: characteristics, mechanisms and experimental study, Int. J. Adv. Manuf. Technol. 93 (9–12) (2017) 3567–3582.
[18] C. A. Loto, "Electrochemical Noise Measurement Technique in Corrosion Research," Int J Electrochem Sci, vol. 7, pp. 9248–9270, 2012, [Online]. Available: www.electrochemsci.org.
[19] L. K. , and H. E. , DeBruyn H., "On-Line Monitoring Using Electrochemical Noise Measurement in CO-CO2-H2O Systems," in Electrochemical Noise Measurement for Corrosion Applications, J. Kearns, J. Scully, P. Roberge, D. Reichert, and J. Dawson, Eds. West Conshohocken: ASTM International, 1996, pp. 214–229.
[20] M. P. Manahan, D. D. Macdonald, and A. J. Peterson, "Determination of the fate of the current in the stress corrosion cracking of sensitized type 304SS in high temperature aqueous systems," Corros Sci, vol. 37, no. 1, 1995.
[21] G. Schmitt, " Fundamental aspects of CO2 metal loss corrosion. Part II: Influence of different parameters on CO2 corrosion mechanism," CORROSION 2015. OnePetro, 2015.
[22] E. Traversa, T. Calderón, Electrochemical investigation on carbon steel behaviour in CO-CO2-H2O environment for the interpretation of the SCC mechanism, Mater. Corros. 42 (1) (1991) 35–40.
[23] K.E. Heusler, G.H. Cartledge, The Influence of Iodide Ions and Carbon Monoxide on the Anodic Dissolution of Active Iron, J. Electrochem. Soc. 108 (1961) 732–740.
[24] F.A. Cotton, G. Wilkinson, Advanced Inorganic Chemistry, Wiley, Chichester, 1980.
[25] D.D. Macdonald, M. Urquidi-Macdonald, A couple environment model for stress corrosion cracking in sensitized type 304 stainles steel in LWR environments, Corros Sci vol. 32, no. l (1991) 51–81.
[26] J.W.V. der Merwe, Environmental and material influences on the stress-corrosion cracking of steel in H-CO-COsolutions, Int. J. Corros. 2012 (2012) 1–14, https://doi.org/10.1155/2012/414156.
[27] S. Pal, R.K. Singh Raman, Determination of threshold stress intensity for chloride stress corrosion cracking of solution-annealed and sensitized austenitic stainless steel by circumferential notch tensile technique, Corros Sci, Jun. 52 (6) (2010) 1985–1991.
[28] R. K. Singh Raman, R. Rihan, R.N. Ibrahim, "Validation of a novel approach to determination of threshold for stress corrosion cracking (KISCC)," Materials Science and Engineering A, vol. 452–453, pp. 652–656, Apr. 2007, doi: 10.1016/j.msea.2006.11.067.
[29] A. Roy, "Stress Corrosion Cracking Tests Using Double-Cantilever-Beam Specimens" (1996).
[30] A.I. Mourad, J. Altarawneha, A.E. Domiaty, Y.J. Chao, F.M. Haggag, Fracture Toughness Measurements From Circumferentially-Notched Pipes Tests, Mater. Perform. Charact. 3 (3) (2014) 305–321.
[31] J.W. Van der Merwe, The effect of the fluctuation of stress on the cracking of steel in aqueous carbon monoxide-carbon dioxide environments, in: 18th International Corrosion Congress, 2012.